Characterization and correction of Global Ozone Monitoring Experiment 2 ultraviolet measurements and application to ozone profile retrievals

Zhaonan Cai,[1] Yi Liu,[1] Xiong Liu,[2] Kelly Chance,[2] Caroline R. Nowlan,[2] Ruediger Lang,[3] Rosemary Munro,[3] and Raid Suleiman[2]

Received 15 November 2011; revised 17 January 2012; accepted 20 February 2012; published 5 April 2012.

[1] We present an assessment study of the Global Ozone Monitoring Experiment 2 (GOME-2) reflectance for the wavelength range 270–350 nm by comparing measurements with simulations calculated using the vector linearized discrete ordinate radiative transfer model (VLIDORT) and Microwave Limb Sounder (MLS) ozone profiles. The results indicate wavelength- and cross-track-position-dependent biases. GOME-2 reflectance is overestimated by 10% near 300 nm and by 15%–20% around 270 nm. Stokes fraction measurements made by onboard polarization measurement devices are also validated directly using the VLIDORT model. GOME-2 measurements agree well with the simulated Stokes fractions, with mean biases ranging from −1.0% to ∼2.9%; the absolute differences are less than 0.05. Cloudiness-dependent biases suggest the existence of uncorrected stray-light errors that vary seasonally and latitudinally. Temporal analysis indicates that reflectance degradation began at the beginning of the mission; the reflectance degrades by 15% around 290 nm and by 2.2% around 325 nm from 2007 through 2009. Degradation shows wavelength- and viewing-angle-dependent features. Preliminary validation of ozone profile retrievals with MLS, Michelson Interferometer for Passive Atmospheric Sounding, and ozonesonde reveals that the application of radiometric recalibration improves the ozone profile retrievals as well as reduces fitting residuals by 30% in band 2b.

Citation: Cai, Z., Y. Liu, X. Liu, K. Chance, C. R. Nowlan, R. Lang, R. Munro, and R. Suleiman (2012), Characterization and correction of Global Ozone Monitoring Experiment 2 ultraviolet measurements and application to ozone profile retrievals, *J. Geophys. Res.*, *117*, D07305, doi:10.1029/2011JD017096.

1. Introduction

[2] The quality of the radiance measured by satellites and the understanding of instrument performance are critical for accurate retrievals of atmospheric trace gases. Absolute calibration of radiance in the ultraviolet (UV) region is essential for retrievals of ozone profiles especially in the troposphere [*Munro et al.*, 1998; *Hoogen et al.*, 1999; *Hasekamp and Landgraf*, 2001; *van der A et al.*, 2002; *Liu et al.*, 2005, 2010a], the absorbing aerosol index (AAI) [*Torres et al.*, 1998], and surface albedo [*Koelemeijer et al.*, 2003; *Kleipool et al.*, 2008]. Both wavelength and radiometric calibrations are important for deriving these geophysical products.

[3] The Meteorological Operational satellite program (Metop), with Metop-A launched in October 2006, is Europe's first polar-orbiting meteorological satellite series. Metop-A flies in a Sun-synchronous polar orbit at 817 km altitude with an equator-crossing time (descending node) of 09:30 local solar time. The Global Ozone Monitoring Experiment 2 (GOME-2) [*European Organisation for the Exploitation of Meteorological Satellites* (*EUMETSAT*), 2006], on board Metop-A, continues monitoring of atmospheric ozone, following on from GOME/ERS-2 and Scanning Imaging Absorption Spectrometer for Atmospheric Chartography (SCIAMACHY)/Envisat [*Bovensmann et al.*, 1999]. GOME-2, as the successor of GOME, is a nadir-viewing spectrometer that scans from east to west and back with a nominal swath width of 1920 km. This instrument measures backscattered radiance in the ultraviolet and visible range (240–790 nm) with a spectral sampling interval of 0.11–0.22 nm and a spectral resolution of 0.24–0.53 nm. Channel 1 (240–315 nm) was divided into two subbands (i.e., bands 1a and 1b) at 307 nm before 10 December 2008 and at 283 nm thereafter. Each forward scan lasts 4.5 s and each backward scan lasts 1.5 s. The nominal integration time for band 1a is 1.5 s, corresponding to three forward ground pixels (640 km × 40 km); band 1b, channel 2 (310–403 nm) and visible channels have an integration time of 0.1875 s, corresponding to 24 forward ground pixels with a maximum resolution of 80 km × 40 km.

[1]Key Laboratory of Middle Atmosphere and Global Environment Observation, Institute of Atmospheric Physics, Chinese Academy of Sciences, Beijing, China.
[2]Harvard-Smithsonian Center for Astrophysics, Cambridge, Massachusetts, USA.
[3]EUMETSAT, Darmstadt, Germany.

0148-0227/12/2011JD017096

[4] The GOME-2 operational level 1b data set contains calibrated Earth radiance, solar irradiance, and polarization measurements derived from raw measurements. The calibrations applied to level 1b data in addition to radiometric calibration include an in-flight spectral calibration, dark-current correction, pixel-to-pixel gain correction, etalon correction, stray-light correction, and a polarization correction [*EUMETSAT*, 2006]. However, some anomalies still exist in the data owing to instrument degradation, applicability of preflight calibration key data, and auxiliary parameters. For GOME, a large reflectance offset in band 1a and radiometric correction problems in the ozone fitting window have been reported [*van der A et al.*, 2002; *Krijger et al.*, 2005a]. Comparison of our preliminary GOME-2 ozone profile retrievals using the GOME and OMI retrieval algorithm [*Liu et al.*, 2005, 2010a] with Microwave Limb Sounder (MLS) ozone profiles showed a large negative bias above the ozone peaks (~25 km), suggesting a reflectance offset at shorter wavelengths.

[5] GOME-2/Metop-A and the GOME-2 instruments to be launched on Metop-B and -C continue monitoring of atmospheric ozone after GOME. They will provide information on ozone, SO_2, and other products for more than 30 years. Thus, study of the instrument degradation and impact on the measurements is critical to the long-term performance of these instruments. GOME measurements have been shown to degrade over time, with Earth radiance and solar irradiance measurements degrading in different ways, leading to degradation in reflectance [*van der A et al.*, 2002; *Krijger et al.*, 2005a; *Liu et al.*, 2007]. Ozone profile retrievals can be significantly affected if reflectance degradation in the ozone fitting window is not considered. The degradation can cause biases of up to 3% and 30% in total column ozone and tropospheric ozone, respectively, for GOME data [*Liu et al.*, 2007]. GOME-2 has a notable loss of throughput (i.e., degradation), especially toward the UV band. The irradiance throughput decreases about 20% per year, which is likely owing to wavelength-dependent degradation of the scan mirror coating and potential contribution from contamination on the detectors. Following an instrument decontamination procedure carried out during one week in September 2009 the throughput of the instrument initially dropped by another 15% [*EUMETSAT*, 2009]. Ozone profile and other products like absorbing aerosol index [*Tilstra et al.*, 2010] using UV channels can be significantly affected by degradation and the reflectance degradation must be corrected.

[6] The purpose of this study is to characterize GOME-2 reflectance by comparing experimental measurements with simulated reflectance calculated using a radiative transfer model. Note that the reflectance is derived using the measured daily irradiance corresponding to the measured radiance. For this purpose, the atmospheric state should be carefully estimated. For wavelengths <350 nm, uncertainties introduced by ground albedo and clouds are relatively small compared with those from ozone [*Tilstra et al.*, 2005], and ozone profiles can be estimated accurately from other collocated and well-validated measurements. In this paper, we focus on the UV region of the spectrum and present a validation study of the reflectance of GOME-2 for the wavelength range of 270–350 nm from February 2007 to December 2009. *Liu et al.* [2010a] validated OMI reflectance and derived an empirical radiometric calibration by comparing measurements with forward model simulations using Aura MLS ozone profiles and ozone profile climatology. We extended and modified this method to validate GOME-2 radiance and polarization measurements in level 1b data. Similar methods for radiance validation have been applied to GOME [*van der A et al.*, 2002; *Krijger et al.*, 2005a] and SCIAMACHY [*Tilstra et al.*, 2005; *van Soest et al.*, 2005] measurements, using different radiative transfer models, spectral precalibration, ozone profile measurements, and other atmospheric state parameters. The Earth's radiance is generally polarized, and therefore the measured signals are of total intensity and the polarized state. Polarization-sensitive instruments such as GOME-2 require polarization correction of radiance. Several methods have been developed to validate GOME and GOME–2 polarization measurements in–flight. One is based on identification of specific geometries for which the light is expected to be unpolarized and another relies on constant limits of polarization in atmosphere [*Aben et al.*, 2003; *Krijger et al.*, 2005b]. In this paper we study the performance of polarization measurements devices of GOME-2 in cloud free conditions with direct radiative transfer model calculations.

[7] In section 2, we describe the GOME-2 level 1b data used in the analysis and details of our simulation method and sensitivity analysis. Section 3 discusses precalibration of the instrument line shape and wavelength shifts in irradiance and radiance spectra. Section 4 characterizes the quality of GOME-2 reflectance using simulated reflectance. We also validate GOME-2 polarization measurement device (PMD) measurements directly with model results. Reflectance degradation is studied and corrected from early 2007 to late 2009. Application of the derived correction to ozone profile retrievals is presented. Section 5 concludes this study.

2. Data and Methods

2.1. GOME-2 Data

[8] The operational calibrated level 1b data are generated by the GOME-2 Product Processing Facility (PPF) from level 1a data, with all calibration steps turned on (dark-signal correction, pixel-to-pixel gain, spectral calibration, etalon correction, polarization correction, and stray-light correction). Level 1b data includes regular solar irradiance measurements over time. Solar spectra are typically acquired once per day at the terminator in the northern hemisphere. The Sun mean reference spectrum will be derived from this mode. The degradation in solar irradiance can be easily monitored by comparing with the solar irradiance measured at the beginning, but it is not easy to tell whether the radiance shows the same reduction and temporal changes as the irradiance. Currently, degradation correction for solar irradiance and earthshine radiance is not included in current versions. In this study, we used 68 days of level 1b spectral data from 16 February 2007 through 16 December 2009, sampled every 15 days. The GOME-2 level 0 to 1b processor was updated to version 4.5 on 9 December 2009. Because the new PPF was applied to only the near-real-time (NRT) data, all data from February 2007 to December 2008 were processed by PPF 4.0, and data from 2009 were processed by versions 4.1 to 4.3. PPF updates are mainly on key data and other issues, which partly improve the data quality (e.g., Stokes fractions). All processor versions up to the most

Table 1. Averaged Estimates of GOME-2 Signal-To-Noise Ratio (SNR) for Orbit 8452 on 15 August 2008

Cross-Track Position	SNR (Mean/Standard Deviation, Min/Max)[a]		
	270–290 nm	290–306 nm	310–350 nm
East	8/6, 2/83	62/59, 10/480	859/329, 10/2851
Nadir	10/7, 2/95	85/93, 7/602	915/404, 34/2531
West	13/9, 2/101	97/88, 7/586	1094/472, 22/2648

[a]The mean and standard deviation are calculated using ground pixels with SZA < 75°.

recent one implemented in March 2011 (version 5.1) have not addressed the issue of changes in reflectance levels due to the observed instrument degradation and stray light.

[9] GOME-2 level 1b PPF data provide the total absolute error (a combination of random and systematic components) in radiance and irradiance measurements [*EUMETSAT*, 2006]. In level 1b data, the total error of irradiance is constant (∼1.42%) and for radiance it is ∼2% above 312 nm. Proper estimate of the random-noise error component of measurements is essential for optimal estimation technique-based algorithms [*Rodgers*, 2000]. Random-noise errors (readout noise and shot noise) of GOME-2 spectra can be estimated from detector counts (original binary units) in the GOME-2 level 1a data. A more convenient way is to convert radiance in level 1b to detector counts using the Müller matrix radiance response elements [*Nowlan et al.*, 2011]. Table 1 lists the averaged signal-to-noise ratio (SNR) values for measured radiance, which can be considered as a measure of the uncertainty (random-noise error) in the measured Earth radiance. Here, we assume that the measured raw spectra were accurately calibrated, so that no uncertainties from calibration key data contributed to the SNR.

[10] The magnitudes of the estimated uncertainties agree well with the standard deviation of spectral fitting residuals for ozone profile and SO_2 retrievals. The relative random-noise error of GOME-2 radiance is ∼0.1% in the range 310–350 nm and increases to 11% in the range 270–290 nm (as seen in Figure 5), with values depending on the signal level resulting from factors such as surface albedo, cloud fraction, solar zenith angle (SZA), and scattering angle. The dependency on scattering angle is quite strong in this wavelength region with low surface albedo (high correlation with the Rayleigh scattering phase function). In addition, the overall accuracy (total error) is also dependent on the scattering angle, for example, errors in the angular dependence of calibration key data. The signal-to-noise ratio decreases as the instrument degradation becomes worse.

2.2. Simulation Method

[11] We compare observed and simulated reflectance spectra for the spectral range 270–350 nm. The reason why we limit the analysis to this window is to understand the GOME-2 instrument calibration for improving ozone profiles and SO_2 retrievals. Simulated spectra are modeled by the vector linearized discrete ordinate radiative transfer model (VLIDORT) [*Spurr*, 2006], a fully linearized multiple scattering radiative transfer model that can simulate the full Stokes vector I, Q (0°/90° polarization), U (±45° polarization), V, and their analytic Jacobians with respect to any atmospheric or surface parameter. VLIDORT can be run in scalar mode only (without polarization), which is faster by almost an order of magnitude than a vector calculation but causes significant errors in the UV. Considering the computational cost of running this vector model, we adopt an optimized scheme to speed up the radiative transfer calculation by a factor of six, while maintaining the accuracy at better than 0.1% [*Liu et al.*, 2010a]. The ring effect, namely, the filling in of solar Fraunhofer lines and telluric absorption structures in the UV/visible due to inelastic rotational Raman scattering (RRS) by air molecules, is directly modeled using a single scattering RRS model [*Sioris and Evans*, 2000], and a scaling parameter is fitted from the observed spectral data to account for multiple scattering effect in the atmosphere. Radiative transfer calculation is performed on a 48 vertical layers grid with approximately 1.5 km thick for each layer. Daily zonal mean ozone profiles are estimated from v2.2 MLS/AURA ozone profiles from 0.1 to 215 hPa and ozone climatology [*McPeters et al.*, 2007] above 215 hPa. These profiles are further normalized by zonal mean OMI total column ozone, which were processed with TOMS algorithm (version 8.5) [*Bhartia and Wellemeyer*, 2002] and have been well validated [*McPeters et al.*, 2008]. Temperature-dependent ozone absorption cross section is taken from *Brion et al.* [1993]. Note that in our forward simulation we account for ozone and Rayleigh scattering to the top of atmosphere. The MLS ozone data were well validated and quality controlled, with uncertainty estimates of ∼5% in the stratosphere, ∼10% at the lowest stratospheric altitudes, and ∼2% in stratospheric column ozone [*Froidevaux et al.*, 2008; *Jiang et al.*, 2007]. Temperature profiles and surface pressures are taken from daily National Centers for Environmental Protection (NCEP) reanalysis data (http://www.ncep.noaa.gov/).

[12] The radiance is calculated for a Rayleigh atmosphere (no aerosols) with Lambertian equivalent reflectance (LER) assumed for the surface and for clouds (treated as reflecting boundaries). Clouds are assumed to be Lambertian surfaces with a reflectivity of 80% and partial clouds are treated as a mixture of clear and cloudy scenes using the Independent Pixel Approximation (IPA). In the IPA, we use the effective cloud top pressure provided in the level 1b data, which is retrieved by FRESCO algorithm [*Koelemeijer et al.*, 2001] from the O2 A band at 762 nm. The initial surface albedo is determined at 347 nm from the OMI surface climatology [*Kleipool et al.*, 2008]. The cloud fraction derivation from 347 nm follows the method of retrieving cloud fraction from weak ozone absorbing wavelengths in the TOMS total ozone algorithm [*Bhartia and Wellemeyer*, 2002] and has been used in our ozone profile retrieval algorithm [*Liu et al.*, 2005, 2010a]. Note that the effective cloud top pressure is also dependent on wavelength [*Stammes et al.*, 2008]. The difference between cloud top derived from O2-A band and rotational Raman scattering near 350 nm are between 2 to 45 hPa [*Sneep et al.*, 2008], which is less than the estimated uncertainty of 53 hPa for FRESCO cloud top retrievals [*Koelemeijer et al.*, 2001]. For near clear sky pixel, the use of inconsistent cloud top pressure will introduce a maximum error of 0.5% near 305 nm assuming 20% cloud and 633 hPa cloud top. We exclude ground pixels flagged as snow/ice by FRESCO. In investigating the zonal mean differences between the observed and simulated reflectance, only ground pixels with effective cloud fractions less than 20%

are included in the average. GOME spectral data are not Nyquist sampled in the spectral domain, which introduces errors when normalizing radiance with irradiance [*Chance et al.*, 2005]. GOME-2 improves the spectral sampling; therefore, an undersampling correction is not implemented.

[13] Over South America and the South Atlantic (0°–45°S, 0°–75°W), the South Atlantic anomaly (SAA) can lead to large measurement spikes in band 1a; thus, the SAA pixels were excluded from the average. We also excluded Sun glint pixels, which can significantly enhance backscattered radiance as well as the polarization state but are not well modeled in our forward model simulation. Scenes or pixels that fulfill all these selection criteria (i.e., nearly clear sky, no SAA, or Sun glint effects) are included in our investigation.

2.3. Forward Model Error and Sensitivity Analysis

[14] We study the sensitivity of modeled reflectance for cloud free scenes in tropics to several forward model parameters: ozone profile, surface albedo and ring effect scaling parameter. We also examine sensitivity to several other parameters that are not included in the model: radiance/O_3 wavelength shift, radiance/irradiance wavelength shift and first-order wavelength-dependent term for surface albedo. The sensitivity of reflectance R to model parameter x is defined as

$$dR^*/dx^* = d\ln(R)/d\ln(x). \quad (1)$$

[15] Derivatives with respect to ozone profile and surface albedo are directly calculated by VLIDORT. Derivatives with respect to wavelength shift and ring effect are derived using the "finite difference" approach. Here we assume that a Lambertian surface is described by albedo that varies linearly with wavelength λ, $A = A_0 + B(\lambda - \bar{\lambda})$. The derivative with respect to the first-order term of albedo is $dR/dB = dR/dA \times (\lambda - \bar{\lambda})$, where A is surface albedo and B is the albedo slope.

[16] In Figure 1a, we present sensitivity of reflectance with respect to Lambertian surface albedo: dR/dA_0 and dR/dB as function of wavelength. Below 300 nm, possible errors in albedo will not affect the simulated reflectance. The effect of albedo increases toward longer wavelengths. The OMI surface albedo data stops at 328 nm, so we assume that the wavelength dependence is small in the forward model, which is a good assumption because the surface albedo is generally small for both land and water surfaces (except for snow/ice surface) and Rayleigh scattering is strong. Assuming wavelength independence, albedo will introduce an error up to 0.9% near 310 nm for water. However, in the ozone profile retrieval algorithm, we fit an additional parameter named "First-order wavelength-dependent term for surface albedo" to account for albedo variation and aerosol effect. Figure 1b shows the sensitivity to ozone profile as a function of wavelength for a typical ozone profile in tropics. Solar zenith angle, viewing zenith angle, and relative azimuth angle are based on a typical GOME-2 pixel on the east side. Above 340 nm, the sensitivity to ozone at all layers is very small. Ozone distribution from ~30 km to bottom layers shows largest impact near 305 nm. The forward model error at shorter wavelengths (<300 nm) is mainly due to errors in ozone profiles. According to *Froidevaux et al.* [2008], the MLS uncertainty estimate is on the order of 5% and closer to 10% at the lowest stratospheric altitudes. The error in simulated reflectance due to uncertainties in MLS data is less than 2%. Figure 1c shows sensitivity of simulated reflectance to the ring effect scaling parameter. Following the method by *Liu et al.* [2010a], we derive the first-order ring spectrum from an independent RRS model [*Sioris and Evans*, 2000]; then a scaling parameter is fitted to account for a small offset in ring spectrum due to multiple scattering. This is done in the first iteration of retrievals before fitting. Although in principle, rotational Raman scattering can be calculated without using fit parameters, the calculation depends on the knowledge of the vertical distribution of ozone, aerosol, clouds, and surface reflection, which are not accurately available.

[17] Other possible error sources are the wavelength shifts between radiance and ozone absorption cross section and between radiance and irradiance, which are not involved in the forward model. Figure 2 presents the calculated sensitivity of the reflectance to the wavelength shifts. Wavelength calibration errors in both radiance and ozone cross-section spectroscopy will introduce some fluctuating structures as seen in Figure 4 and will be discussed in section 4.1. Thermally induced shift and possibly squeeze may occur between irradiance and radiance, in addition to the Doppler shift from acquisition of irradiances when the substantial spacecraft velocity vector is mostly in the Earth-Sun direction, which has already been corrected in level 0–1b processing. Wavelength adjustment between radiance and irradiance is needed when calculating reflectance, which will introduce additional errors as seen in Figure 2b. We did not shift irradiance and radiance during the simulation because the retrieved wavelength shift (section 3) produces highly variable values depending on the pixel window used and does not make improvement. In the ozone retrieval algorithm, we further fit radiance/irradiance shift parameters to account for residual wavelength registration errors.

3. Precalibration of the Slit Function

[18] A preflight instrument study found GOME-2 slit functions to be quite asymmetric in channels 1 and 2, especially for the shorter part of band 2b [*Siddans et al.*, 2006]. Here, we assume a variable (wavelength-dependent) asymmetric Gaussian slit shape for convolving high-resolution spectra to GOME-2 spectral resolution. The prefitted slit widths (full width at half maximum, FWHM), wavelength shift, and asymmetric factor were retrieved by nonlinear least squares (NLLS) fitting of the observed irradiance spectrum with an improved high-resolution (0.04 nm) solar reference spectrum, which has a wavelength accuracy better than 3.2×10^{-4} above 305 nm and better than 3×10^{-3} below 305 nm [*Chance and Kurucz*, 2010]. The asymmetric Gaussian $\boldsymbol{g(x)}$ is defined as

$$g(x) = \exp\left(\frac{x^2}{(hw1e \cdot (1 \pm aym))^2}\right), \quad (2)$$

where x is the difference in wavelengths, $hw1e$ is half width at 1/e intensity, FWHM = 1.66511 × $hw1e$, and aym is the asymmetry factor.

[19] To account for variable slit width, we prefit the slit width over a spectral range of 31 pixels with a sliding step

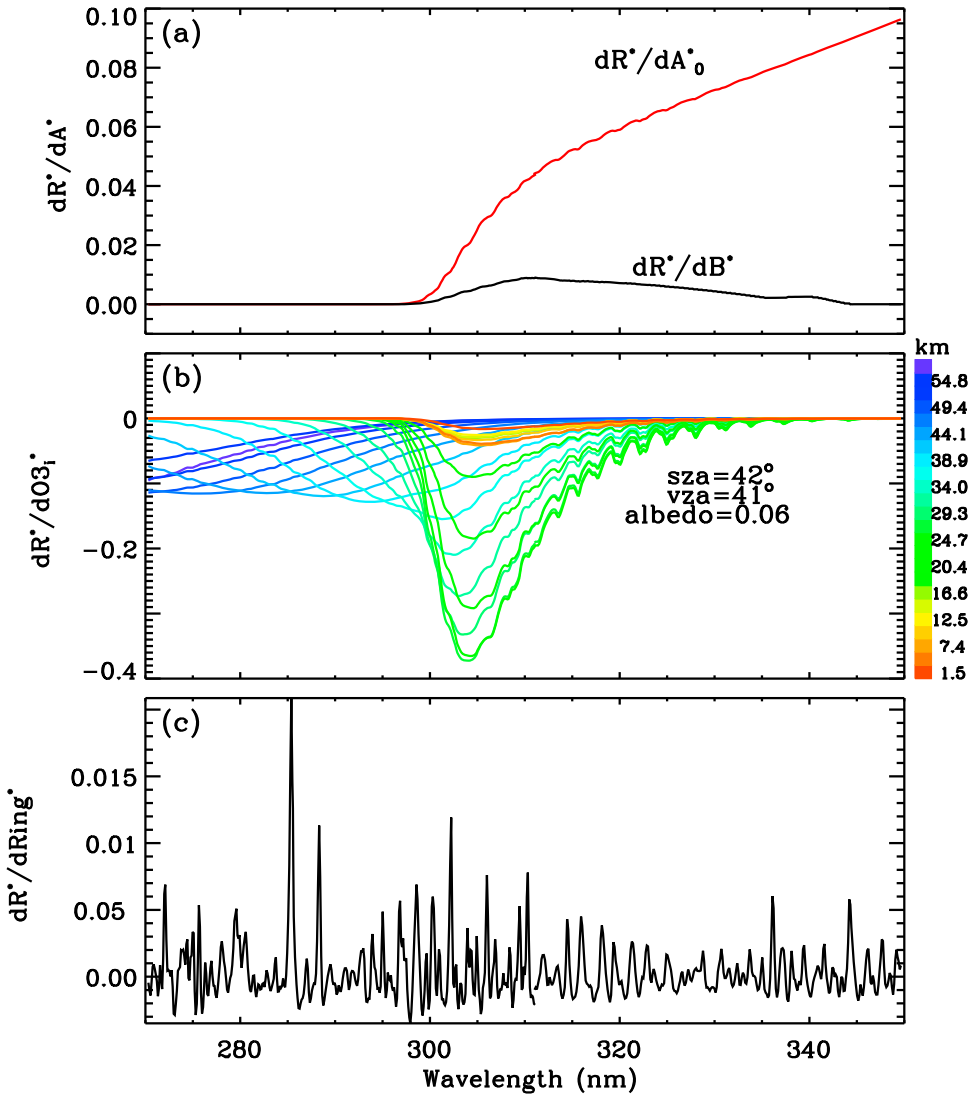

Figure 1. Sensitivity of the reflectance to (a) Lambertian surface albedo: zero-order and first-order term; (b) typical ozone profile ($O3_i$), where subscript i denotes layer or altitude and different altitudes are shown in different colors; and (c) ring effect scaling parameter as a function of wavelength, on 15 August 2008. For these cases, SZA = 42° and viewing zenith angle (VZA) = 41°, which corresponds to eastside pixel for one GOME-2 scan (see Figure 3).

size of 1 pixels increment. The fitting procedure includes baseline and scaling polynomials that can partly account for systematic errors like those due to stray light. Figure 3a shows an example of slit widths (FWHM) and asymmetry factor retrieved from GOME-2 irradiance spectra on 15 August 2008. The retrieved slit widths, similar to preflight measurements (red line) [*Siddans et al.*, 2006], vary less with wavelength in both channels 1 and 2 compared with GOME, where slit width varies substantially with wavelength in the Huggins bands [*Liu et al.*, 2005]. The much larger slit widths than the preflight measurements around 280 nm may be due to errors around this strong Fraunhofer region. The slit width changes with time decreasing by 6% from 2007 to 2009. The fitting residuals of ozone profiles and SO_2 for GOME-2 are reduced using the retrieved slit shape. GOME-2 spectra are acquired by linear photodiode array detectors, and operational wavelength calibration is performed by the spectral light source (SLS), which provides a number of narrow spectral lines at known wavelengths across the GOME-2 wavelength range [*Murray*, 1994]. We examined the wavelength shifts for irradiance spectra and earthshine radiance spectra. Figure 3b gives an example of fitted wavelength shifts for solar irradiance and radiance in the range of 270–350 nm measured on 15 August 2008. GOME-2 shows wavelength-dependent variation similar to GOME: large wavelength shifts in the overlap region of channel 1 and channel 2 (i.e., the end of band 1b (309–314 nm) and the beginning of band 2b (310–315 nm)); large fluctuations for radiance shift in the range of 313–323 nm. However, the fluctuating structures of solar irradiance have much smaller amplitudes than those of GOME. We do not perform a wavelength adjustment on individual radiance spectra owing to overall similar shifts between radiance and irradiances. In addition, this does not improve fitting residuals. In the

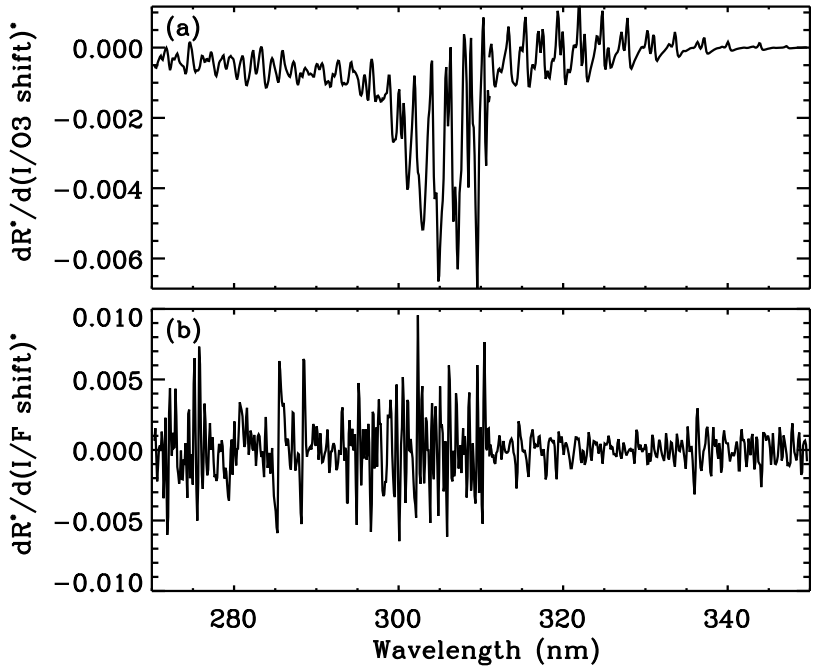

Figure 2. Sensitivity of the reflectance to (a) wavelength shift between radiance and ozone cross section and (b) radiance/irradiance wavelength shift.

retrieval, we fit a relative radiance/irradiance shift parameter, that is, we calculated the reflectance as the ratio of radiance to shifted irradiances. The fitted radiance/irradiance shifts are usually very small, within 0.005 nm.

4. Reflectance and Polarization Comparison

[20] We examine average differences between observed (R_{obs}) and simulated (R_{sim}) reflectance for each cross-track position, spectrally and temporally. The relative difference of N selected pixels, d_R, is defined as

$$d_R = \frac{1}{N}\sum_{i=1}^{N}(R_{obs} - R_{sim})/R_{sim} \times 100. \quad (3)$$

[21] The measurement uncertainties have to be reduced by increasing the number of comparison spectra, especially below 290 nm. We focus on comparisons over the tropics (25°S–5°N) where there is less ozone variation. For each cross-track position on each day, 400–900 measurements are averaged to ensure that most of the longitudes are covered, in order to minimize the effect of zonal variability in ozone and to average out the variation due to measurement uncertainty. We also compare the Stokes fraction polarization measurements made by GOME-2 with modeled simulation results. To identify the reflectance degradation in GOME-2 data, we compared the reflectance from February 2007 through December 2009. Because of the large computational effort involved, we only apply this comparison every 15 days during the 3 year period. We also examine the comparison globally for several days from different seasons.

4.1. Spectrum Comparison

[22] Figure 4 shows an example of a comparison between R_{obs} and R_{sim} as a function of wavelength in the wavelength range of 270–350 nm on 15 August 2008. Strong wavelength- and cross-track-position (scanning angle)-dependent biases indicate the existence of radiometric calibration problems including instrument degradation in the GOME-2 data. Below 300 nm, the GOME-2 reflectance is typically overestimated by 8–25% compared with the simulation, which are too large to be explained by error in the forward model. Below 289 nm, d_R had a strong correlation (0.4–0.8) with the averaged radiance of band 1a (270–307 nm), as well as with the cloud fraction, suggesting the existence of uncorrected uniform stray light. The correlation also shows cross-track and latitude dependencies (e.g., weaker correlation for west and lower solar zenith angle pixels). Spikes at 280 and 285 nm (280 nm is an Mg+ or Mg II Fraunhofer line, 285 nm is a neutral Mg Fraunhofer line) are likely caused by the emission of Mg and Mg+ in the ionosphere and residual stray light [*Joiner and Aikin*, 1996], which are not modeled in the forward simulation. Radiances below 300 nm are scattered back to the instrument through single scattering and have low sensitivity to tropospheric clouds, aerosols, and surface albedo, owing to the strong ozone absorption. Thus, the polarization can be modeled accurately, and most likely the cross-track-dependent biases cannot be explained by errors in the polarization correction; this is discussed further in section 4.2. The fine structures at shorter wavelengths, especially below 290 nm, are likely caused by metal emission lines (e.g., Mg, Fe), NO gamma emission features, and stray light filling in Fraunhofer lines.

[23] The discontinuity in the overlap region (310–313 nm) of bands 1b and 2b varies from 7% in the western/eastern positions to 3.5% at nadir. In band 2b, the observed reflectance near 312 nm is higher than the simulation by 3%, whereas by 310 nm, the difference is larger than 10%. These are possible effects of the missing Etalon correction below 315 nm. The fluctuating structures in band 2b have a strong

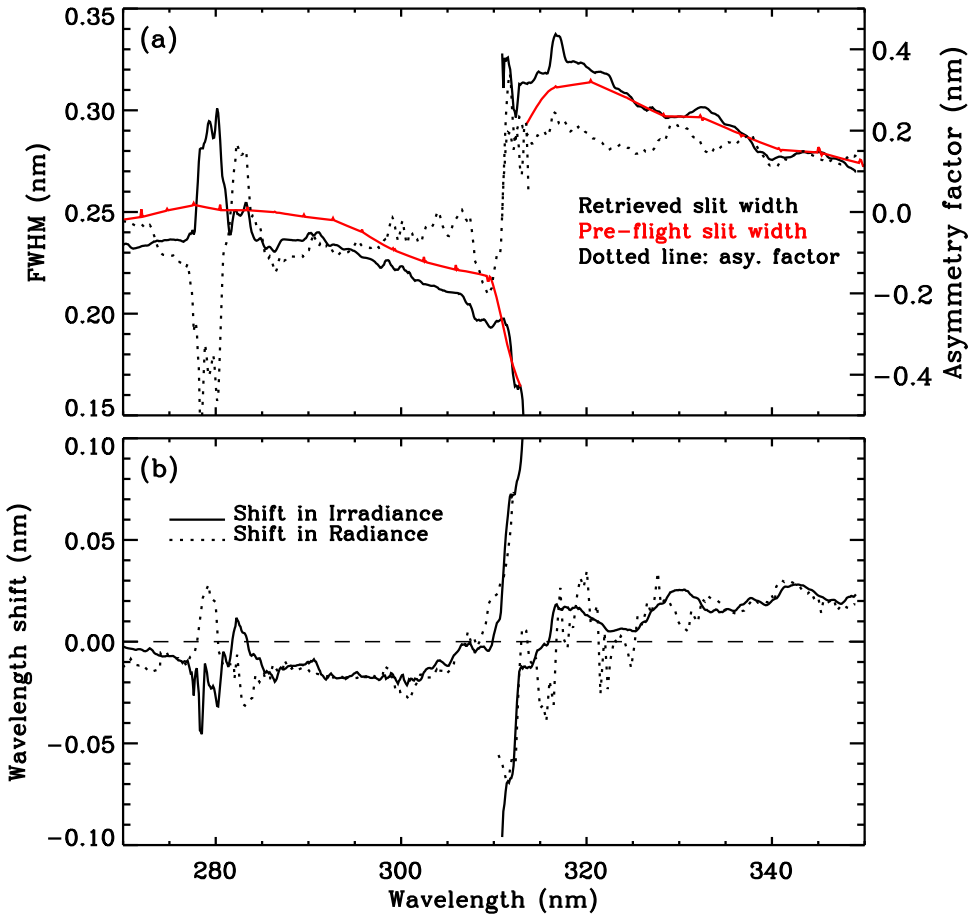

Figure 3. (a) Retrieved GOME-2 slit widths and asymmetry factors in the range 270–350 nm, averaged from 96 spectra during 2007–2009. Red lines denote slit widths from calibration key data. (b) One example of GOME-2 wavelength shifts for irradiance (solid line) and radiance (dashed line) in the range 270–350 nm for a pixel on 15 August 2008.

correlation (0.5–0.7) with the wavelength shift between radiance and ozone cross sections and a weaker correlation (∼0.3) with the wavelength shift between irradiance and radiance and the residual ring effect. The stronger correlation between ozone cross sections and radiance suggests a relative wavelength shift rather than a wavelength calibration error because of the weak correlation with radiance/irradiance wavelength shifts, which were fitted in our simulation. These wavelength shifts introduced features indicate wavelength calibration problems in level 1b data or in ozone cross sections and can be removed by smoothing the spectra with a running average of 1 or 2 nm.

[24] On the basis of the methodology described in section 2, reflectance correction is derived for GOME-2 level 1b spectra. Figure 5 shows the mean difference and 3σ standard deviation of 68 d_R spectra during 2007–2009 for all scans under nearly clear sky condition (effective cloud faction <20%). Eight band 1b and 2b spectra are coadded to match the band 1a integration time (spatial resolution). Biases for different days show similar structures (not shown here), but the magnitudes vary substantially with wavelength, time, and cross-track positions. The mean biases (deviation) vary from 18% (18%) at 270 nm to <0.1% (0.1%) at 347 nm. At longer wavelengths, the small biases result from the cloud fraction determination so that differences close to 347 nm are minimized. The absolute error provided by the level 1b product is based on the assumption of zero degradation and no systematic error in the stray-light characterization of the instrument and the radiance errors estimated in this study are mainly due to degradation and stray light. As a comparison, we also plot total absolute error in the level 1b data and estimated random noise in Figure 5. The absolute errors in radiance are almost constant (∼2%), above 312 nm and do not vary much with time and cross-track position. Note that in Figure 5, the value is 1.6% because it is a combination of irradiance and radiance errors and 8 band 2b pixels have been coadded to match band 1a integration time.

4.2. Polarization Comparison

[25] The GOME-2 PMDs measure light polarized parallel and perpendicular to the reference plane in 15 broad bands from 312 to 790 nm, from which the Stokes fraction $\boldsymbol{q}$ = Q/I can be determined. For comparison, we used VLIDORT to calculate $\boldsymbol{q}$ directly and evaluate radiance biases due to the polarization correction. This is done for four PMD wavelengths (312.7, 318.0, 325.3, and 332.6 nm, corresponding to PMDs 1, 2, 3, and 4) in the Huggins ozone absorption band. We also examine the differences at 298 nm. GOME-2

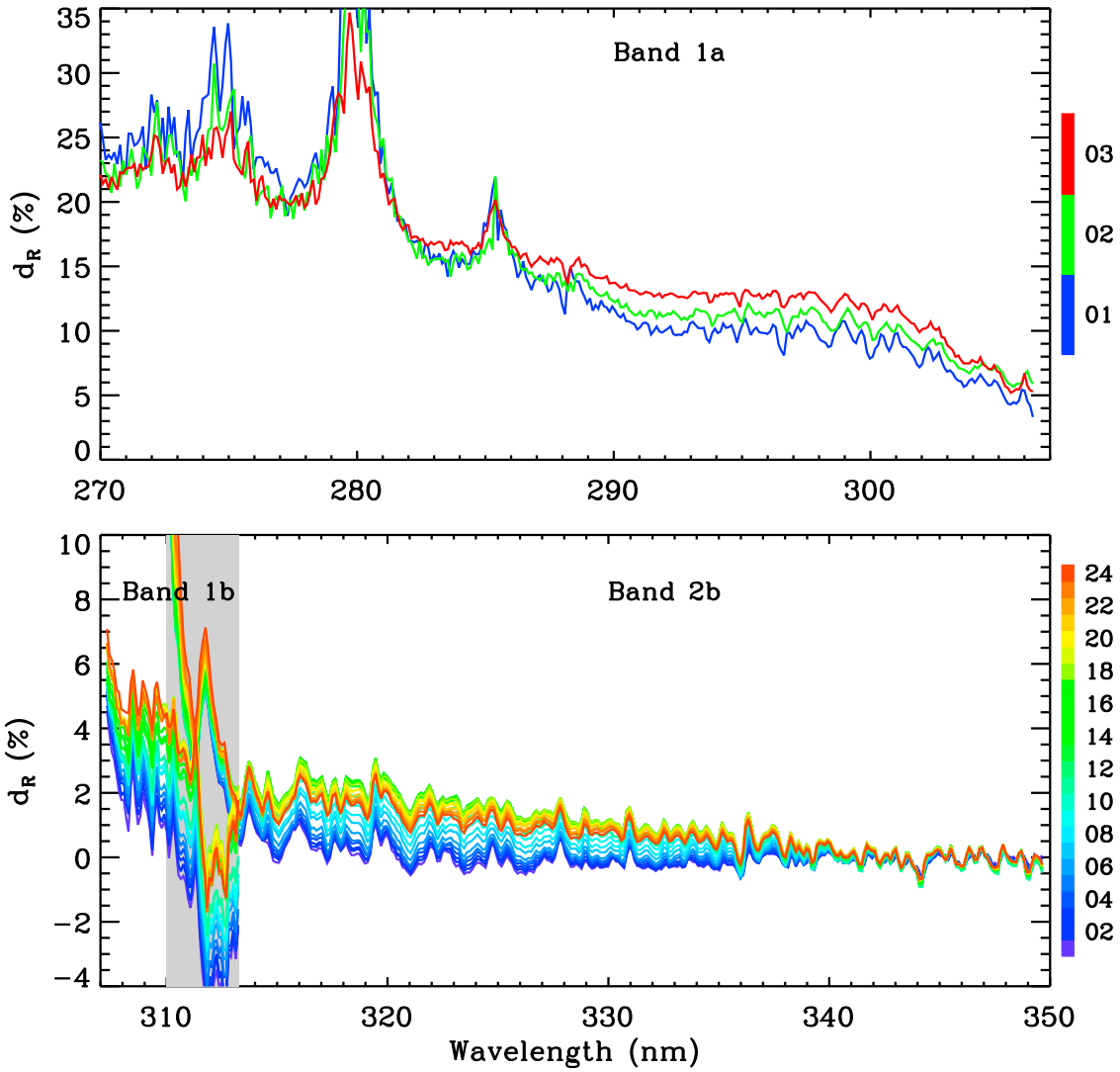

Figure 4. Average relative differences between observed and simulated reflectance spectra for part of bands 1a, 1b, and 2b as a function of wavelength. Different cross-track positions are shown in different colors. Numbers 1, 2, and 3 in the top plot correspond to east, nadir, and west pixels, respectively. These residuals are derived from nearly clear sky scenes (effective cloud fraction less than 20%) in the latitude band from 25°S to 5°N on 15 August 2008. Pixels affected by the South Atlantic anomaly, snow/ice, and Sun glint are excluded. The shaded area marks the overlap region of bands 1b and 2b.

does not measure polarization at this wavelength. Because only single scattering contributed to $\boldsymbol{q}$, the $\boldsymbol{q}$ value in level 1b data is actually based on theoretical single scattering calculation [*EUMETSAT*, 2006]. Pixels with $\boldsymbol{q}$ values within ±0.05 are not used in order to avoid singularities. The threshold 0.05 is artificially selected following the GOME-2 polarization correction determination algorithm in which the polarization sensitivity of the instrument with respect to the U Stokes component was equivalently set to zero when the single-scattering Stokes fraction ($\boldsymbol{q_{ss}}$) is smaller than 0.05 [*EUMETSAT*, 2006].

[26] Figure 6a shows the zonal mean absolute differences between observed and simulated $\boldsymbol{q}$ for 298 nm for three band 1a cross-track positions and for PMDs 1, 2, 3, and 4 for different band 2b cross-track positions in the same spectral region as shown in Figure 4. These values depend on cross-track position and wavelengths, and range between −0.03 and 0.05. The effect of errors in the Stokes fraction $\boldsymbol{q}$ on the reflectance are estimated by calculating errors in the polarization correction factor $\boldsymbol{c}$, defined as [*EUMETSAT*, 2006]

$$c = 1 + q\left(\mu^2 + \frac{u_{ss}}{q_{ss}}\mu^3\right), \tag{4}$$

where μ^2 and μ^3 describe the polarization sensitivity of the instrument with respect to the Q and U Stokes components, respectively. Here $\boldsymbol{q_{ss}}$ is the Stokes fraction (0°/90°) for Rayleigh single scattering, and $\boldsymbol{u_{ss}}$ is the Stokes fraction (−45°/+45°) for Rayleigh single scattering; errors in $\boldsymbol{c}$ can be estimated from $c_{sim}-c_{obs}$. Instrument signals or detector counts are polarization corrected by dividing them by $\boldsymbol{c}$. As shown in Figure 6b, those errors are typically between −0.2% and 0.3% for the wavelengths and cross-track positions we investigated, indicating that polarization correction

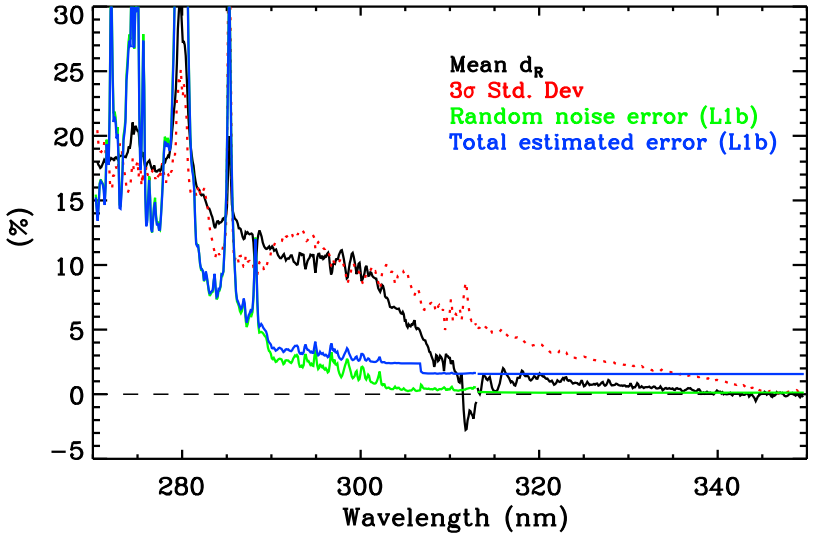

Figure 5. Similar to Figure 4 but for mean differences (solid line) and 3σ standard deviation (dotted line) of the 68 dR spectra from February 2007 to December 2009. Eight band 1b and 2b spectra are coadded to match the band 1a resolution. Also plotted are the mean total absolute error (blue) in GOME-2 level 1b data and random-noise error (green) calculated from the method described in section 2.1.

errors contribute only a small portion to the biases shown in Figure 4 and that the cross-track-position-dependent bias cannot be explained by these errors.

[27] The Stokes fraction q in the Huggins band (300–330 nm) is very sensitive to tropospheric ozone. The inclusion of polarization information in addition to UV radiance information can increase tropospheric ozone sensitivity, mainly in the free and upper troposphere [*Hasekamp and Landgraf*, 2002], and reduce the dependence on viewing geometry [*Liu et al.*, 2009]. The potential for using the GOME-2 PMDs to improve tropospheric ozone retrievals is of great interest. Figure 7 shows a scatterplot of GOME-2 $\boldsymbol{q}$

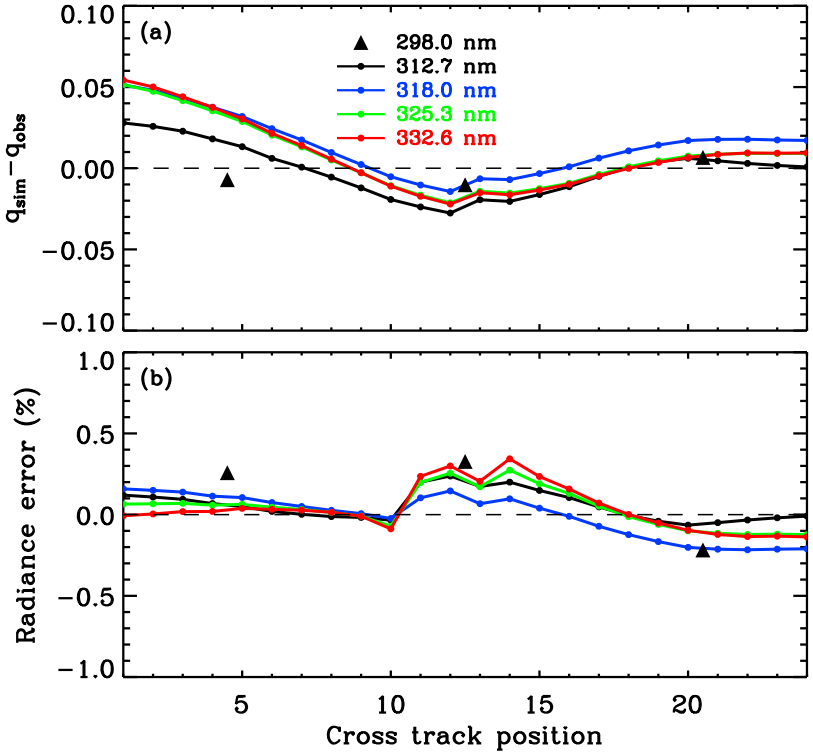

Figure 6. (a) Mean absolute differences of the Stokes fraction $\boldsymbol{q}$ between GOME-2 ($\boldsymbol{q}_{obs}$) data and simulations ($\boldsymbol{q}_{sim}$) for 298.0, 312.7, 318.0, 325.3, and 332.6 nm (corresponding to PMDs 1, 2, 3, and 4) as a function of cross-track position. (b) Similar to Figure 6a but for the effect of error in the Stokes fraction on reflectance.

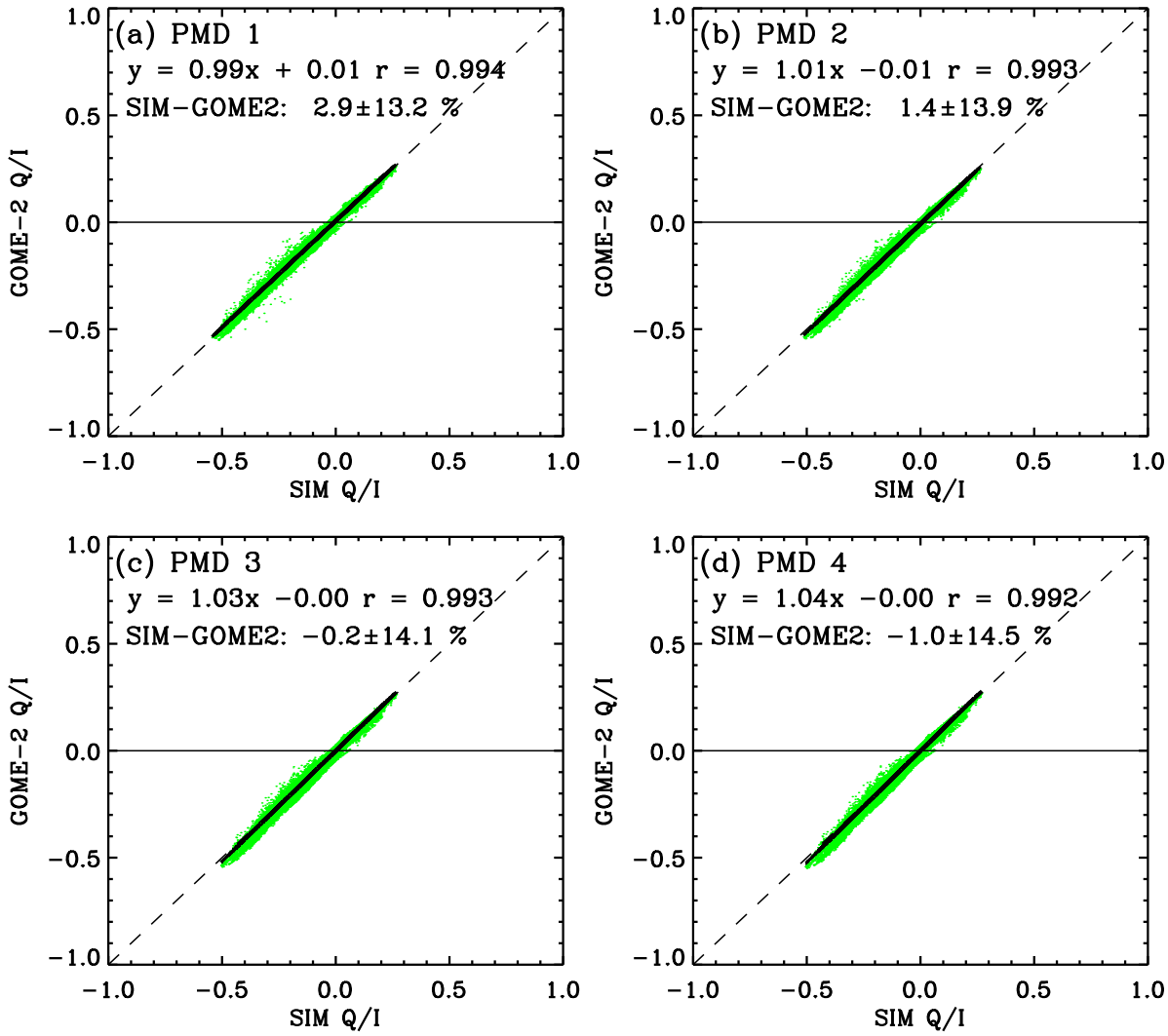

Figure 7. Scatterplots of the GOME-2 Stokes fraction q versus simulations for four PMD channels at 312.7, 318.0, 325.3, and 332.6 nm on 15 August 2008. GOME-2 pixels were selected in the same manner as that used for Figure 4. The solid and dashed lines denote the linear regression and 1:1 relationship, respectively. The slope, offset, correlation, mean difference, and 1σ standard deviation are also shown.

versus those simulations for PMD channels 1, 2, 3, and 4, derived for clear-sky conditions on 15 August 2008. GOME-2 correlates well with the simulations (r > 0.99, N = 32,303). The slopes are close to one, with values ranging from 0.99 to 1.04. There is scatter between GOME-2 and the simulated q. The deviations are due to errors in the climatological tropospheric ozone and the exclusion of aerosols in the forward model simulation. The mean biases, which minimize errors due to ozone zonal variability, are 2.9% for PMD 1 and −1.0% for PMD 4. The mean absolute differences in q (similar to Figure 6a, but averaged globally) are within ±0.05 and show similar cross-track-position dependencies as those shown in Figure 6a. Similar values have been found by examining the angular dependency of Stokes fractions for special viewing geometries (where q should be close to zero) [*EUMETSAT*, 2008]. For highly polarized cloud-free cases, PMD measurements are verified with accuracy better than 2.9%, and no cloud-fraction-dependent bias is found. For low-polarized measurements, neither observations nor model simulations represented Stokes fractions very well; they do not improve ozone profile retrievals owing to little information content.

4.3. Spatial Comparison

[28] To understand the spatial variations of anomalies in reflectance, we examine the spectrally averaged residuals for two wavelength ranges, 270–290 nm ($d_{R(270–290)}$) and 320–340 nm ($d_{R(320–340)}$), as a function of latitude on 15 January, 15 April, 16 July, and 16 October 2008. The spikes at 276, 280, 285, and 288 nm are excluded. In Figure 8, for clear conditions (effective cloud fraction <20%), $d_{R(270–290)}$ varies less than 5% with latitude, and $d_{R(320–340)}$ is constant over most latitudes. For cloudy conditions (effective cloud fraction >40%), peaks of $d_{R(270–290)}$ occur in the tropics are likely due to the presence of more reflective deep convective clouds. For wavelengths shorter than 290 nm, $d_{R(270–290)}$, which was thought to be insensitive to the presence of clouds, increases with increasing cloudiness, suggesting that

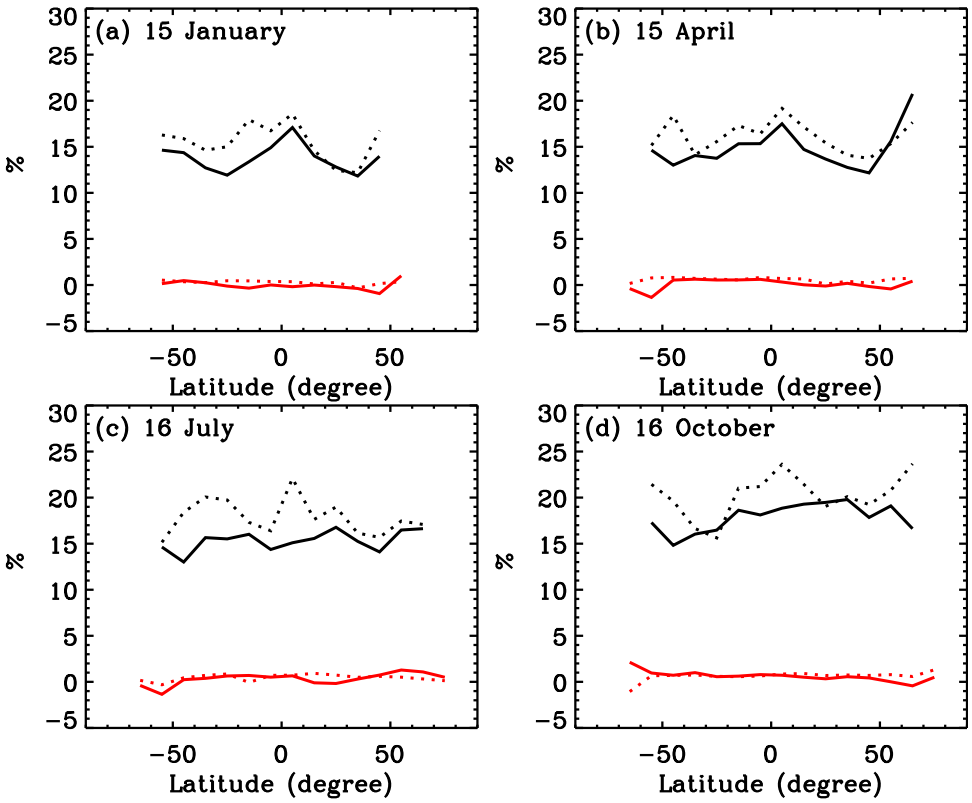

Figure 8. Spectrally averaged relative differences between GOME-2 data and simulated reflectance for four days in 2008 as a function of latitude, in two wavelength windows: 270–290 nm (black lines) and 320–340 nm (red lines). Solid lines show differences derived from clear-sky conditions (effective cloud fraction <20%), and dotted lines show differences derived from cloudy conditions (effective cloud fraction >40%). Pixels affected by the South Atlantic anomaly, snow/ice, and Sun glint were excluded.

there are residual uniform stray-light errors in band 1a, and that these errors depend on the intensity level (e.g., depend on scattering angle, surface albedo, and SZA). For $d_{R(320-340)}$, no distinct difference between clear and cloudy conditions is found. Although there are errors in MLS and climatological ozone in the simulations, sample errors, and errors in cloud parameters, the overall features indicate that the radiometric correction derived in the tropics could be applied to other latitudes. Residual stray-light errors vary seasonally and latitudinally and should be corrected independently or fitted in the retrieval.

4.4. Reflectance Degradation

[29] For GOME and SCIAMACHY, several empirical methods have been developed to correct reflectance degradation by comparing observed and simulated reflectance [*van der A et al.*, 2002; *Krijger et al.*, 2005a; *van Soest et al.*, 2005] or by comparing the observed reflectance with that at the start after removing dependences on the SZA and seasonal variation [*Liu et al.*, 2007]. These methods suffer from several disadvantages: First, simulation methods require careful collocations of independent ozone measurements such as ozonesondes and ozone profile data from other instruments. However, there are generally not enough collocations. Second, the method of comparing the observed reflectance with that at the beginning of instrument operation does not remove the change in reflectance due to ozone variation and could not detect and correct any initial offset in the measurements.

[30] Figure 9 shows a temporal analysis of the zonal mean differences between observed and simulated reflectance for two wavelengths, 290 nm and 325 nm, in our ozone profile fitting window derived from nearly clear sky conditions (cloud fraction less than 20%) in the tropics during the study period (2007–2009). The increasing values indicate the existence of wavelength-dependent degradation in the GOME-2 reflectance. The overall characteristics are similar to those of GOME in the first 3 years in orbit. For GOME, the degradation is quite small up to 1999 [*Liu et al.*, 2007]. The degradation began in 2007 and is expected to be nonlinear with time, as observed in GOME. The cross-track dependent slopes indicate that reflectance degradation significantly depends on viewing angle (e.g., the east pixels degraded less than nadir and west pixels), with first-order values ranging from 3% to 15% at 290 nm and 0.6% to less than 2.2% at 325 nm after 3 years. On the basis of the GOME experience, the physical understanding of the scan-angle-dependent degradation is that the scan mirror's reflective properties, due to contamination, depend strongly on the incident angle [*Snel*, 2000]. Our approach mainly derives the wavelength- and cross-track-position-dependent part of the radiance errors, so degradation for longer wavelengths cannot be fully identified since we derived cloud fractions from 347 nm, which forced the measurement/simulation ratio to be equal to one. However, degradation rates decreased thereafter from 20% to below 5% per year in

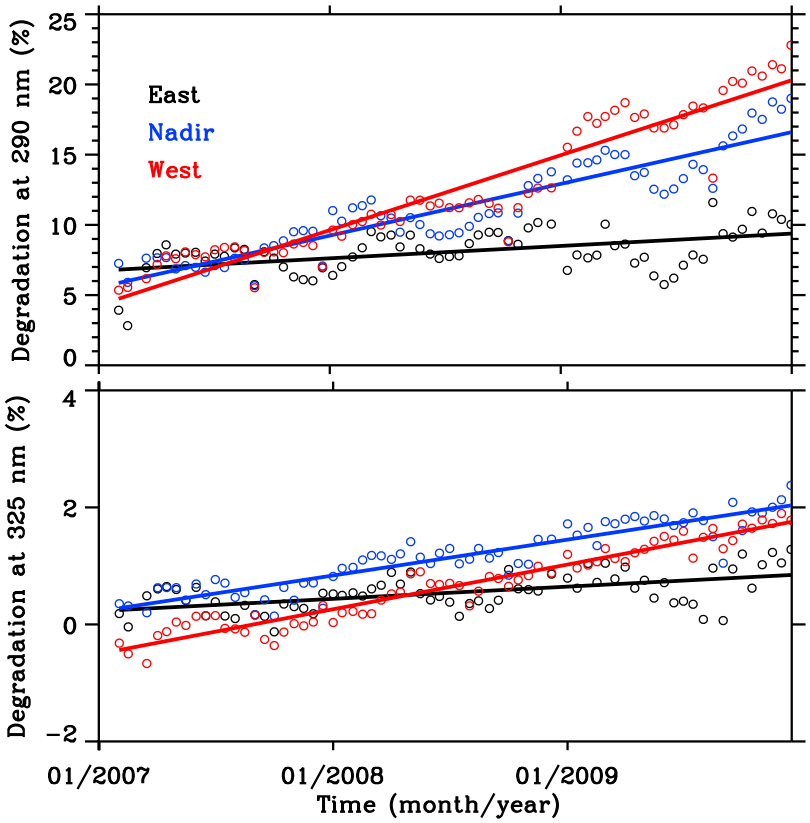

Figure 9. Mean differences between observed and simulated reflectance for (top) 290 nm versus time and (bottom) 325 nm versus time. The band 1a cross-track positions are shown in different colors for east (black), nadir (blue), and west (red), respectively. First-order fitted lines are also shown.

the UV with virtually no degradation in the visible and NIR region during 2010.

[31] The derived degradation correction has some disadvantages. First, the effective cloud fraction was fitted at wavelengths around 347 nm from uncorrected measurements; thus, error in the derived cloud fraction directly propagates into the simulated spectra, which reduces the biases at longer wavelengths [*Krijger et al.*, 2005a]. So the ratio of simulated reflectance to observed reflectance at longer wavelengths might not reflect the absolute calibration. However, for ozone profile retrievals, the wavelength-dependent radiometric calibration is more important. Second, sampling (68 days) and modeling errors (e.g., zonal mean ozone, climatology) remain, as does instrument uncertainty.

4.5. Application to Ozone Profile Retrievals and Validation

4.5.1. Example of Reflectance Correction

[32] On the basis of the comparison between measured and simulated radiance, radiometric recalibration of reflectance as a function of wavelength, cross-track position, and time is derived. To validate the derived correction, we apply recalibrated GOME-2 radiance in our ozone profile retrieval algorithm [*Liu et al.*, 2005, 2010a]. We choose fitting windows of 289–307 nm and 325–340 nm. Figure 10 shows the effect of the correction on GOME-2 ozone profile retrievals. GOME-2 ozone profile retrievals with and without radiometric correction are compared with coincident MLS and the a priori profile at MLS layers (0.3–215 hPa) for 1 August 2008, globally. Coincident GOME-2 and MLS ozone profiles are selected to be <300 km in space and 6 h in time. The total number of coincident pairs is 632. The comparison process is similar to that used by *Liu et al.* [2010b]. The MLS ozone volume mixing ratio recorded at each pressure level record is integrated to partial columns (in Dobson units, DU), and then MLS profiles are convolved with GOME-2 averaging kernels to reduce the smoothing error. For profile comparison, GOME-2 ozone profiles are interpolated to the MLS vertical grid. For clarity, the Dobson units are converted to parts per million by volume (ppmv). The uncorrected retrievals show a negative bias above 22 hPa, decreasing to −18% near 2 hPa, and positive biases up to 10% at bottom levels. The radiometric correction improves the comparison with MLS at all layers above 215 hPa. GOME-2 agrees with MLS to within 3.5% from 0.3 to 215 hPa. The standard deviations are within 8%, increasing to 20% near 215 hPa. Additionally, the correction reduced fitting residuals in band 2b by ~30%. The large deviations in bottom layers were largely due to ozone variability in the upper troposphere and lower stratosphere (UTLS) region and uncertainty from MLS precision (green dashed line, Figure 10). Large differences between corrected and uncorrected profiles near 2 hPa are due to the radiance offset below 300 nm.

[33] The "soft" calibration is also implemented in GOME-2 SO_2 retrieval [*Nowlan et al.*, 2011] and improves the SO_2 retrieval by (1) improving cross-track-dependent bias, (2) improving SO_2 background offset retrieved in clean

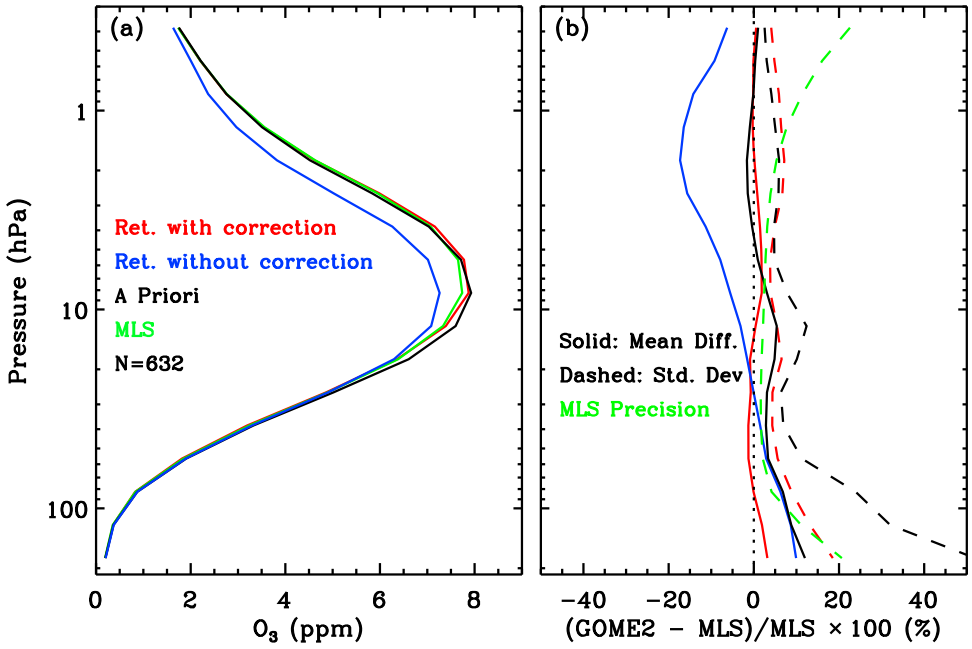

Figure 10. (a) Comparison of retrieved GOME-2 ozone profiles with (red) and without (blue) reflectance correction, MLS (green), and the a priori profile (black). (b) Mean bias (solid line) and standard deviation (dashed line) at MLS layers on 1 August 2008. MLS profiles are convolved with GOME-2 averaging kernels; the green dashed line shows MLS precision.

environment by 0.5–1 DU, (3) reducing large systematic residuals in the normalized log of radiance by a factor of 4 in the wavelength range below 320 nm, and (4) allowing a retrieval combining both channels 1 and 2, which can be used to reduce retrieval noise in later years after degradation, as well as permitting altitude retrievals of high-altitude SO_2 plumes, whose weighting functions peak at shorter wavelengths than those at lower altitudes [*Yang et al.*, 2010].

4.5.2. Validation of Ozone Profile With Michelson Interferometer for Passive Atmospheric Sounding Ozone Data

[34] The Michelson Interferometer for Passive Atmospheric Sounding (MIPAS) is a limb scanning Fourier

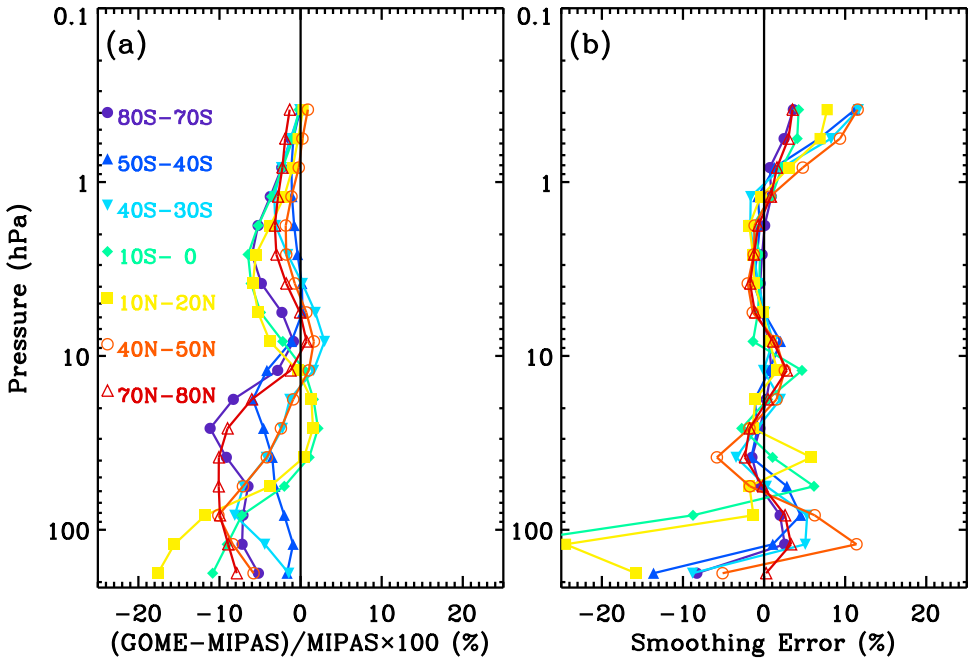

Figure 11. (a) Mean bias between GOME-2 and MIPAS convolved with GOME-2 averaging kernels at each MIPAS layer for seven 10°-latitude bands during 2008. (b) Corresponding smoothing errors.

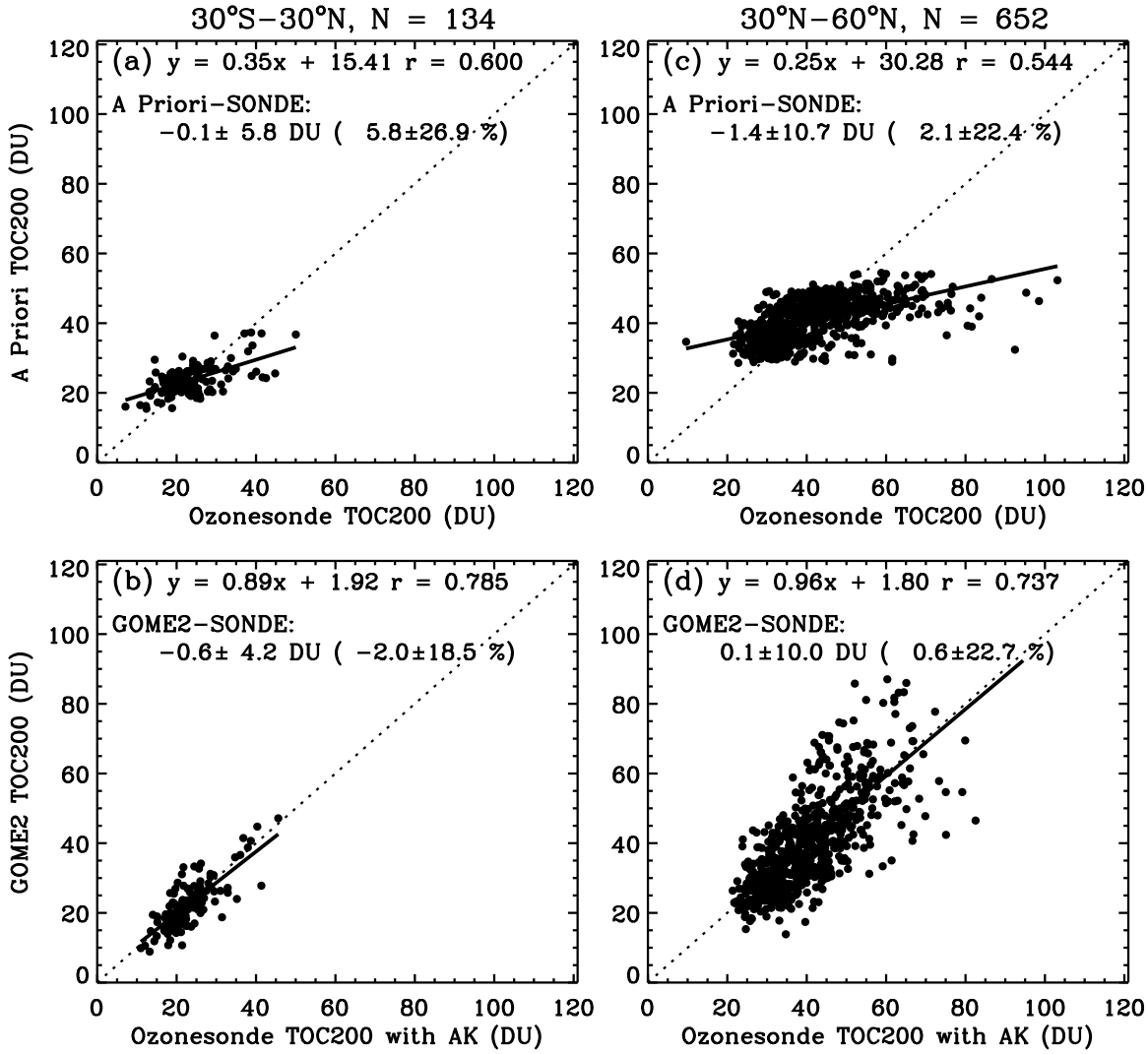

Figure 12. Comparison of tropospheric ozone column from surface to 200 hPa (TOC200) between retrievals/a priori and ozonesondes: (a, b) tropics (30°S–30°N) and (c, d) midlatitude (30°N–60°N) during 2008. Figures 12a and 12c show a priori TOC200 versus ozonesonde. Figures 12b and 12d show GOME-2 TOC200 versus ozonesonde. The solid and dashed lines denote the linear regression and 1:1 relationship, respectively. The number of coincident profiles, slope, offset, correlation, mean difference, and 1σ standard deviation are also shown.

infrared spectrometer on board the European Environmental Satellite (Envisat) in March 2002. The instrument was suspended in March 2004 owing to problems with the mirror drive of the interferometer and restarted in January 2005 with a degraded spectral resolution of 0.0625 cm^{-1} and measurement scenario to extend instrument life time. The horizontal sampling step is 410 km in normal mode and vertical sampling step is 1.5 km to 4 km with vertical range of 7 to 70 km. MIPAS ozone profiles are obtained for most of the stratosphere during both daytime and nighttime hours. MIPAS ozone data shows consistent error less than 10% from 1 hPa to 50 hPa and 5–25% around 100 hPa [*Cortesi et al.*, 2007; *Ceccherini et al.*, 2008]. Here we use MIPAS operational near real time data of processor version 5.05.

[35] Figure 11 shows the mean biases of differences between GOME-2 and MIPAS ozone profiles for seven latitude bands from 80°S to 80°N during 2008 and corresponding smoothing errors. The comparison process is same as that is section 4.5.1. GOME-2 agrees well with MIPAS with biases less than 10% except for large values at bottom layers which are likely due to degradation in the quality of MIPAS in the lower stratosphere and upper troposphere [*Cortesi et al.*, 2007] and, as already noticed, to the large ozone gradients in the UTLS region. The mean smoothing errors, estimated by assuming MIPAS as true, are generally within 3% except for several layers below 1 hPa (∼10%) and above 80 hPa (up to 25%). The biases show similar characteristics as the results of the comparison for MIPAS reduced-spectral-resolution measurements with Global Ozone Monitoring by Occultation of Stars (GOMOS) data [*Ceccherini et al.*, 2008]. Biases between MIPAS and GOME-2 show similar magnitude of values (negative biases up to 10%) as the comparison of MIPAS and MLS in the stratosphere [*Froidevaux et al.*, 2008; *Chauhan et al.*, 2009].

4.5.3. Validation of Tropospheric Ozone Column With Ozonesondes

[36] We validate GOME-2 tropospheric ozone column (TOC) (Surface to 200 hPa, TOC200) retrievals with ozonesonde for the tropics (30°S–30°N) and midlatitudes (30°N–60°N) during 2008. We only use retrievals with effective cloud fraction <50% and sondes with correction factors between 0.5 and 1.5. The collocation criteria are 500 km in space and 8 h in time. Ozonesonde data are from the World Ozone and Ultraviolet Data Centre (WOUDC, http://www.woudc.org) including stations from 30°S to 60°N and the station at Beijing (116°28′E, 39°48′N). The ozonesonde launched at Beijing is developed by the Institute of Atmospheric Physics (IAP) of the Chinese Academy of Sciences (CAS) and has been launching for almost ten years since 2002. Ozonesonde of different type have different precisions, and accuracies measurements with different types of ozonesondes are typically within 10–20% with respect to the accurate UV photometer measurements. Precision of electrochemical concentration cell (ECC) sondes is 5% and sondes of Brewer Mast and carbon iodine are 10–15% [*World Meteorological Organization*, 1998].

[37] Figure 12 compares tropospheric ozone column from the surface to 200 hPa between GOME-2, a priori and ozonesonde. To remove smoothing errors, ozonesonde profiles are convolved with GOME-2 averaging kernels (AK). The retrieval mainly improves the slope, offset and correlation over the a priori. In the tropics, the mean biases and standard deviation between GOME-2 and sondes are -0.6 ± 4.2 DU ($2.0 \pm 18.5\%$), and the correlation is 0.785. The retrieved TOC improves the mean bias in the tropics. In midlatitudes, the mean biases and standard deviation between GOME-2 and sondes are 0.1 ± 10.0 DU ($0.6 \pm 22.7\%$) with correlation 0.737. The large standard deviation is possibly due to errors in both measurements and assumed parameters in the algorithm and spatiotemporal variation since the GOME-2 spatial resolution is 640 km × 40 km. The comparison also shows seasonal/SZA dependent biases (not shown here) which indicate errors due to residual stray-light errors and radiative transfer calculation errors. In addition, the "soft" calibration reduces systematic biases in observed reflectance but there are remaining errors especially in the degradation correction due to sampling, which will introduce some seasonal dependent biases.

5. Conclusions

[38] The GOME-2 reflectance is characterized and corrected by comparing experimental and simulated data for the wavelength range of 270–350 nm. The simulations are calculated with VLIDORT, zonal mean MLS ozone profiles, and ozone climatology. The GOME-2 reflectance shows significant wavelength- and cross-track-dependent biases ranging from −5 to 25%, especially at shorter wavelengths. For the overlap region of channels 1 and 2, the cross-track-position-dependent discontinuity ranges from 3.5 to 7%. Wavelength shifts introduce high-resolution structures in band 2b, suggesting the need for additional wavelength calibration. Spatial comparison shows that the derived reflectance correction in band 2b is constant with varying latitude as well as the SZA. In band 1a, uncorrected stray light remains, varying seasonally and latitudinally. Temporal analysis indicates that GOME-2 reflectance degrades over time by 3–15% for 290 nm and by less than 2.2% for 325 nm from 2007 to 2009. The degradation depends on wavelength and scan angle. Long-term degradation still needs to be investigated. The radiance error identified is a combination of errors in radiometric calibration and radiative transfer modeling, as well as of assumptions that go into the forward modeling. Although there are errors from forward model parameters (e.g., temperature profiles, ozone cross section, reference spectra, MLS ozone, ozone climatology, and the OMI total ozone column) and there are differences due to PPF versions, the overall features suggest problems in radiometric calibration. We also verify polarization measurements (Stokes fractions) observed by GOME-2 directly with modeled values in the ozone Huggins absorption band. For highly polarized cases, the observed Stokes fractions agree well with simulations, with mean biases ranging from −1.0 to 2.9%.

[39] We have derived a first-order correction to GOME-2 radiance in the UV using average difference between measured and simulated reflectance in the tropics. This "soft" calibration is presented as a function of wavelength, cross-track position, and time. We apply the correction independent of latitude. Comparisons of ozone retrievals with and without radiometric correction and MLS ozone profiles verify that the derived reflectance correction can improve retrieved ozone profiles, and reduce fitting residuals by 30% in band 2b. The GOME-2 level 1b data have in some sense been calibrated to MLS, so we validate the accuracy of final ozone profile retrievals with independent MIPAS and ozonesondes measurements. The retrieved ozone profiles and tropospheric ozone column from recalibrated GOME-2 level 1b data agree well with these data. The soft calibration derived from this study can be obtained from the first author and will be updated with the process PPF of GOME-2.

[40] **Acknowledgments.** This study was supported by the National Science Foundation of China under grant 41075014 and the Public Meteorology Special Foundation of MOST (grant GYHY201106045). Research at the Smithsonian Astrophysical Observatory was funded by NASA and the Smithsonian Institution. We thank EUMETSAT for providing GOME-2 level 1 data and the OMI science team, MLS science team, and WOUDC for providing the satellite data and ozonesonde data. We thank C. G. Wang, H. B. Chen, and C. J. Bian for providing ozonesonde data at Beijing. We also thank R. J. D. Spurr for providing the VLIDORT code.

References

Aben, I., C. P. Tanzi, W. Hartmann, D. M. Stam, and P. Stammes (2003), Validation of space-based polarization measurements by use of a single-scattering approximation, with application to the Global Ozone Monitoring Experiment, *Appl. Opt.*, *42*(18), 3610–3619, doi:10.1364/AO.42.003610.

Bhartia, P. K., and W. C. Wellemeyer (2002), TOMS-V8 total O3 algorithm, in *OMI Ozone Products*, vol. 2, *OMI Algorithm Theoretical Basis Document*, edited by P. K. Bhartia, pp. 51–73, NASA Goddard Space Flight Cent., Greenbelt, Md.

Bovensmann, H., J. P. Burrows, M. Buchwitz, J. Frerick, S. Noël, V. V. Rozanov, K. V. Chance, and A. P. H. Goede (1999), SCIAMACHY: Mission objectives and measurement modes, *J. Atmos. Sci.*, *56*, 127–150, doi:10.1175/1520-0469(1999)056<0127:SMOAMM>2.0.CO;2.

Brion, J., A. Chakir, D. Daumont, J. Malicet, and C. Parisse (1993), High-resolution laboratory absorption cross section of O_3: Temperature effect, *Chem. Phys. Lett.*, *213*(5–6), 610–612, doi:10.1016/0009-2614(93)89169-I.

Ceccherini, S., U. Cortesi, P. T. Verronen, and E. Kyrölä (2008), Technical note: Continuity of MIPAS-ENVISAT operational ozone data quality from full- to reduced-spectral-resolution operation mode, *Atmos. Chem. Phys.*, *8*(8), 2201–2212, doi:10.5194/acp-8-2201-2008.

Chance, K., and R. L. Kurucz (2010), An improved high-resolution solar reference spectrum for Earth's atmosphere measurements in the ultraviolet, visible, and near infrared, *J. Quant. Spectrosc. Radiat. Transfer*, *111*(9), 1289–1295, doi:10.1016/j.jqsrt.2010.01.036.

Chance, K., T. P. Kurosu, and C. E. Sioris (2005), Undersampling correction for array detector-based satellite spectrometers, *Appl. Opt.*, *44*(7), 1296–1304, doi:10.1364/AO.44.001296.

Chauhan, S., et al. (2009), MIPAS reduced spectral resolution UTLS-1 mode measurements of temperature, O_3, HNO_3, N_2O, H_2O and relative humidity over ice: Retrievals and comparison to MLS, *Atmos. Meas. Tech.*, *2*(2), 337–353, doi:10.5194/amt-2-337-2009.

Cortesi, U., et al. (2007), Geophysical validation of MIPAS-ENVISAT operational ozone data, *Atmos. Chem. Phys.*, *7*(18), 4807–4867, doi:10.5194/acp-7-4807-2007.

European Organisation for the Exploitation of Meteorological Satellites (EUMETSAT) (2006), GOME-2 Level 1 product generation specification, *EPS.SYS.SPE.990011*, Darmstadt, Germany.

European Organisation for the Exploitation of Meteorological Satellites (EUMETSAT) (2008), GOME-2 PMD band definitions 3.0 and PMD calibration, *EUM/OPS-EPS/DOC/07/0601*, Darmstadt, Germany.

European Organisation for the Exploitation of Meteorological Satellites (EUMETSAT) (2009), GOME-2 FM3 long-term in-orbit degradation: Status after 2nd throughput test, *EUM.OPS-EPS.TEN.09.0318*, Darmstadt, Germany.

Froidevaux, L., et al. (2008), Validation of Aura Microwave Limb Sounder stratospheric ozone measurements, *J. Geophys. Res.*, *113*, D15S20, doi:10.1029/2007JD008771.

Hasekamp, O. P., and J. Landgraf (2001), Ozone profile retrieval from backscattered ultraviolet radiances: The inverse problem solved by regularization, *J. Geophys. Res.*, *106*(D8), 8077–8088, doi:10.1029/2000JD900692.

Hasekamp, O. P., and J. Landgraf (2002), Tropospheric ozone information from satellite-based polarization measurements, *J. Geophys. Res.*, *107*(D17), 4326, doi:10.1029/2001JD001346.

Hoogen, R., V. Rozanov, and J. Burrows (1999), Ozone profiles from GOME satellite data: Algorithm description and first validation, *J. Geophys. Res.*, *104*(D7), 8263–8280, doi:10.1029/1998JD100093.

Jiang, Y. B., et al. (2007), Validation of Aura Microwave Limb Sounder Ozone by ozonesonde and lidar measurements, *J. Geophys. Res.*, *112*, D24S34, doi:10.1029/2007JD008776.

Joiner, J., and A. C. Aikin (1996), Temporal and spatial variations in upper atmospheric Mg+, *J. Geophys. Res.*, *101*(A3), 5239–5249, doi:10.1029/95JA03517.

Kleipool, Q. L., M. R. Dobber, J. F. de Haan, and P. F. Levelt (2008), Earth surface reflectance climatology from 3 years of OMI data, *J. Geophys. Res.*, *113*, D18308, doi:10.1029/2008JD010290.

Koelemeijer, R., P. Stammes, J. Hovenier, and J. D. Haan (2001), A fast method for retrieval of cloud parameters using oxygen A band measurements from the Global Ozone Monitoring Experiment, *J. Geophys. Res.*, *106*(D4), 3475–3490, doi:10.1029/2000JD900657.

Koelemeijer, R. B. A., J. F. de Haan, and P. Stammes (2003), A database of spectral surface reflectivity in the range 335–772 nm derived from 5.5 years of GOME observations, *J. Geophys. Res.*, *108*(D2), 4070, doi:10.1029/2002JD002429.

Krijger, J. M., I. Aben, and J. Landgraf (2005a), CHEOPS-GOME: WP2.1: Study of instrument degradation, *SRON-EOS/RP/05–018*, Eur. Space Agency, Paris.

Krijger, J. M., C. P. Tanzi, I. Aben, and F. Paul (2005b), Validation of GOME polarization measurements by method of limiting atmospheres, *J. Geophys. Res.*, *110*, D07305, doi:10.1029/2004JD005184.

Liu, X., K. Chance, C. E. Sioris, R. J. D. Spurr, T. P. Kurosu, R. V. Martin, and M. J. Newchurch (2005), Ozone profile and tropospheric ozone retrievals from the Global Ozone Monitoring Experiment: Algorithm description and validation, *J. Geophys. Res.*, *110*, D20307, doi:10.1029/2005JD006240.

Liu, X., K. Chance, and T. P. Kurosu (2007), Improved ozone profile retrievals from GOME data with degradation correction in reflectance, *Atmos. Chem. Phys.*, *7*(6), 1575–1583, doi:10.5194/acp-7-1575-2007.

Liu, X., P. K. Bhartia, K. Chance, and R. J. D. Spurr (2009), Monitoring of tropospheric ozone from backscattered ultraviolet/visible measurements on geostationary platforms, *Eos Trans. AGU*, *90*(52), Fall Meet. Suppl., Abstract A53A-0243.

Liu, X., P. K. Bhartia, K. Chance, R. J. D. Spurr, and T. P. Kurosu (2010a), Ozone profile retrievals from the Ozone Monitoring Instrument, *Atmos. Chem. Phys.*, *10*(5), 2521–2537, doi:10.5194/acp-10-2521-2010.

Liu, X., P. K. Bhartia, K. Chance, L. Froidevaux, R. J. D. Spurr, and T. P. Kurosu (2010b), Validation of Ozone Monitoring Instrument (OMI) ozone profiles and stratospheric ozone columns with Microwave Limb Sounder (MLS) measurements, *Atmos. Chem. Phys.*, *10*(5), 2539–2549, doi:10.5194/acp-10-2539-2010.

McPeters, R. D., G. J. Labow, and J. A. Logan (2007), Ozone climatological profiles for satellite retrieval algorithms, *J. Geophys. Res.*, *112*, D05308, doi:10.1029/2005JD006823.

McPeters, R., et al. (2008), Validation of the Aura Ozone Monitoring Instrument total column ozone product, *J. Geophys. Res.*, *113*, D15S14, doi:10.1029/2007JD008802.

Munro, R., R. Siddans, W. J. Reburn, and B. J. Kerridge (1998), Direct measurement of tropospheric ozone distributions from space, *Nature*, *392*(6672), 168–171, doi:10.1038/32392.

Murray, J. E. (1994), Atlas of the spectrum of a platinum/chromium/neon hollow-cathode reference lamp in the region 240–790 nm, report, Eur. Space Agency, Paris.

Nowlan, C. R., X. Liu, K. Chance, Z. Cai, T. P. Kurosu, C. Lee, and R. V. Martin (2011), Retrievals of sulfur dioxide from the Global Ozone Monitoring Experiment 2 (GOME-2) using an optimal estimation approach: Algorithm and initial validation, *J. Geophys. Res.*, *116*, D18301, doi:10.1029/2011JD015808.

Rodgers, C. D. (2000), *Inverse Methods for Atmospheric Sounding: Theory and Practice*, World Sci., Hackensack, N. J.

Siddans, R. B. J. K., B. G. Latter, J. Smeets, G. Otter, and S. Slijkhuis (2006), Analysis of GOME-2 slit function measurements: Final report, *EUM/CO/04/1298/RM*, Eur. Organ. for the Exploit. of Meteorol. Satell., Darmstadt, Germany.

Sioris, C., and W. Evans (2000), Impact of rotational Raman scattering in the O_2 *A* band, *Geophys. Res. Lett.*, *27*(24), 4085–4088, doi:10.1029/2000GL012231.

Sneep, M., J. F. de Haan, P. Stammes, P. Wang, C. Vanbauce, J. Joiner, A. P. Vasilkov, and P. F. Levelt (2008), Three-way comparison between OMI and PARASOL cloud pressure products, *J. Geophys. Res.*, *113*, D15S23, doi:10.1029/2007JD008694.

Snel, R. (2000), In-orbit optical path degradation: GOME experience and SCIAMACHY prediction, paper SP-461 presented at ERS Envisat Symposium, Eur. Space Agency, Göteborg, Sweden.

Spurr, R. J. D. (2006), VLIDORT: A linearized pseudo-spherical vector discrete ordinate radiative transfer code for forward model and retrieval studies in multilayer multiple scattering media, *J. Quant. Spectrosc. Radiat. Transfer*, *102*(2), 316–342, doi:10.1016/j.jqsrt.2006.05.005.

Stammes, P., M. Sneep, J. F. de Haan, J. P. Veefkind, P. Wang, and P. F. Levelt (2008), Effective cloud fractions from the Ozone Monitoring Instrument: Theoretical framework and validation, *J. Geophys. Res.*, *113*, D16S38, doi:10.1029/2007JD008820.

Tilstra, L. G., G. van Soest, and P. Stammes (2005), Method for in-flight satellite calibration in the ultraviolet using radiative transfer calculations, with application to Scanning Imaging Absorption Spectrometer for Atmospheric Chartography (SCIAMACHY), *J. Geophys. Res.*, *110*, D18311, doi:10.1029/2005JD005853.

Tilstra, L. G., O. N. E. Tuinder, and P. Stammes (2010), GOME-2 absorbing aerosol index: Statistical analysis, comparison to GOME-1 and impact of instrument degradation, paper presented at 2010 Meteorological Satellite Conference, Eur. Organ. for the Exploit. of Meteorol. Satell., Darmstadt, Germany.

Torres, O., P. Bhartia, J. Herman, Z. Ahmad, and J. Gleason (1998), Derivation of aerosol properties from satellite measurements of backscattered ultraviolet radiation: Theoretical basis, *J. Geophys. Res.*, *103*(D14), 17,099–17,110, doi:10.1029/98JD00900.

van der A, R. J., R. F. van Oss, A. J. M. Piters, J. P. F. Fortuin, Y. J. Meijer, and H. M. Kelder (2002), Ozone profile retrieval from recalibrated Global Ozone Monitoring Experiment data, *J. Geophys. Res.*, *107*(D15), 4239, doi:10.1029/2001JD000696.

van Soest, G., L. G. Tilstra, and P. Stammes (2005), Large-scale validation of SCIAMACHY reflectance in the ultraviolet, *Atmos. Chem. Phys.*, *5*(8), 2171–2180, doi:10.5194/acp-5-2171-2005.

World Meteorological Organization (1998), SPARC/IO3C/GAW assessment of trends in the vertical distribution of ozone, *Rep. 43*, Global Ozone Res. and Monit. Proj., Geneva, Switzerland.

Yang, K., X. Liu, P. K. Bhartia, N. A. Krotkov, S. A. Carn, E. J. Hughes, A. J. Krueger, R. J. D. Spurr, and S. G. Trahan (2010), Direct retrieval of sulfur dioxide amount and altitude from spaceborne hyperspectral UV measurements: Theory and application, *J. Geophys. Res.*, *115*, D00L09, doi:10.1029/2010JD013982.

Z. Cai and Y. Liu, Key Laboratory of Middle Atmosphere and Global Environment Observation, Institute of Atmospheric Physics, Chinese Academy of Sciences, Beijing 100029, China. (liuyi@mail.iap.ac.cn)

K. Chance, X. Liu, C. R. Nowlan, and R. Suleiman, Harvard-Smithsonian Center for Astrophysics, Cambridge, MA 02138, USA.

R. Lang and R. Munro, EUMETSAT, D-64295 Darmstadt, Germany.